

diffraction. The two satellites on either side of an a-type reflection have similar intensity.

With reflections which have strong satellites, sharp quasi-periodic boundaries parallel to (0001) are in good contrast in dark-field micrographs (Fig. 6). The boundaries, spaced at 30 Å (corresponding to the distance between the two satellites), are disrupted across the {10 $\bar{1}$ 4} structure, which appears as diffuse dark and light regions. Streaking parallel to c^* indicates that faults are not strictly periodic, which is evident from the morphology of the pattern.

The occurrence of satellites in the diffraction pattern of dolomite documents a new superstructure in this mineral. The superstructure contains a basal stacking which is different from that of ideal dolomite and the faults imaged in Fig. 6 could represent periodic antiphase domain boundaries (APB) with a morphology very similar to that of metamorphic intermediate plagioclase (14). Nonconservative APB's can be due to cation ordering from a disordered state, but in the case of dolomite it is more likely that they formed during replacement growth. They appear to be an expression of non-stoichiometry with extra layers of Ca intercalated in the structure (7). In fact, the crystals under consideration are Ca-rich ($\text{Ca}_{0.54}\text{Mg}_{0.46}\text{CO}_3$) as determined by microprobe analysis. Other possibilities are a different stacking of anion layers or a combination of cation and anion stacking. At this stage the evidence is insufficient to identify the true structure and we must await results from high-resolution microscopy.

The basal stacking superstructure has been found in all crystals in the net fabric, both in euhedral crystals growing in the calcite cells and in the subhedral crystals in the seams evolving from replacement along stylolites. It is present equally in all stages of replacement, including samples in which dolomite has completely replaced calcite, suggesting that physicochemical conditions and mechanisms of dolomitization were similar throughout. It appears that basal defects represent structures formed during deep burial replacement and that the original dolomite structure was probably not disordered "protodolomite" (15, 16) but contains a different type of ordering than "ideal" dolomite. The prominent growth form of the dolomite crystals in the studied samples is $r = \{10\bar{1}4\}$. The Lost Burro crystals also provide a clear example of late diagenetic replacement of consolidated limestone, both along stylolites and directly in the matrix.

Locally, Mg must have migrated to the

site of nucleation along stylolites, now-healed microfractures, and crystal boundaries. The unique occurrence, morphology, and microstructure of these samples add complexity to the "dolomite problem" (17, 18) and encourage more systematic surveys of sedimentary dolomites with the transmission electron microscope. Heretofore, little has been done in this regard, and most of the work has been on low-temperature dolomites (1, 2). Specifically, the geologic significance of the new dolomite superstructure needs to be explored to determine more precisely the conditions leading to its formation. We have begun to study the extent of dolomite with satellites in the Lost Burro Formation away from the limestone-dolomite contacts. Such study bears on the questions of pervasiveness and operating mechanisms of burial dolomitization.

H. R. WENK

Department of Geology and
Geophysics, University of California,
Berkeley 94720

D. H. ZENGER

Department of Geology,
Pomona College,
Claremont, California 91711

References and Notes

1. R. J. Reeder and H. R. Wenk, *Geophys. Res. Lett.* **6**, 77 (1979).
2. R. J. Reeder, *Contrib. Mineral. Petrol.* **76**, 148 (1981).
3. S. H. Gunderson and H. R. Wenk, *Am. Mineral.* **66**, 789 (1981).
4. H. R. Wenk and S. Frisia-Bruni, *Geol. Soc. Am. Abstr. Programs* **14** (No. 7) (1982).
5. L. S. Land, *Sedimentology* **20**, 411 (1973).
6. P. A. Sandberg, *ibid.* **22**, 495 (1975).
7. J. R. Goldsmith and D. L. Graf, *Am. Mineral.* **43**, 84 (1958).
8. J. Van Landuyt and S. Amelinckx, *ibid.* **60**, 351 (1975).
9. D. H. Zenger, in *Geology of Selected Areas in the San Bernardino Mountains, Western Mojave Desert, and Southern Great Basin, California: Guidebook and Volume, Field Trip 9, Cordilleran Section*, J. D. Cooper, B. W. Troxel, L. A. Wright, Eds. (Cordilleran Section Meeting, Geological Society of America, Anaheim, Calif., 1982), pp. 129-136.
10. D. H. Zenger, *Geology*, in press.
11. B. W. Mattes and E. W. Mountjoy, *Soc. Econ. Paleontol. Mineral. Spec. Publ.* **28** (1980), pp. 259-297.
12. D. W. Morrow, *Geosci. Can.* **9**, 95 (1982).
13. Cover page, *Am. Assoc. Pet. Geol. Bull.* **66** (No. 1) (1982).
14. H. R. Wenk and Y. Nakajima, *Phys. Chem. Miner.* **6**, 169 (1980).
15. A. M. Gaines, *Science* **183**, 518 (1974).
16. D. L. Graf and J. R. Goldsmith, *J. Geol.* **64**, 173 (1956).
17. R. W. Fairbridge, "Regional aspects of carbonate deposition," *Soc. Econ. Paleontol. Mineral. Spec. Publ.* **5** (1957), pp. 124-178.
18. G. V. Chilingar, D. H. Zenger, H. J. Bissell, K. H. Wolf, *Dev. Sedimentol.* **25A**, 423 (1979).
19. Supported by NSF grant 7823848 (to H.R.W.) and American Chemical Society, Petroleum Research Fund, grants 13615-AC2 (to H.R.W.) and 2678-B2 (to D.H.Z.).

20 October 1982; accepted 17 June 1983

Satellite Detection of Effects Due to Increased Atmospheric Carbon Dioxide

Abstract. *The use of satellites to detect climatic changes due to increased carbon dioxide was investigated. This method has several advantages over ground-based methods of monitoring climatic change. Calculations indicate that, by monitoring the outgoing longwave flux for small intervals in the 15-micrometer spectral region, changes in stratospheric temperatures due to doubled atmospheric carbon dioxide are large enough to be detected above the various sources of noise. This method can be extended to other spectral regions so that causal links between changes in outgoing longwave radiation due to other trace gases and the thermal structure of the atmosphere could be established.*

Various methods have recently been proposed to detect a climatic signal due to increased atmospheric CO₂ (1). Most of these methods involve studying surface climatic variables (surface temperature, sea levels, area of ice coverage, and so forth), which are strongly affected by a myriad of atmospheric, oceanic, and cryospheric processes. The methods cannot establish any causal connection between observed changes in a climatic variable and changes in the radiative balance of the earth-atmosphere system, and they are limited in their spatial and temporal coverage, which in turn limits the sample size used to determine a climatic change.

One climatic variable that is easily measured on a global scale is the long-

wave flux emitted at the top of the atmosphere. The amount of energy emitted at any given spectral interval depends on the atmospheric temperature structure as well as on the amount and distribution of absorbers. Any increase in atmospheric CO₂ will lead to an increase in the opacity of the earth's atmosphere and thus to an alteration in the spectral distribution of outgoing energy (2).

To estimate the magnitude of this change in a selected spectral region, we performed a series of calculations to determine the outgoing flux of energy in the 500 to 800 cm⁻¹ spectral region. This region, centered around 15 μm, contains the CO₂ band system that is most important for studies of increased CO₂. Most of the emission of longwave radiation

from this spectral region originates in the stratosphere. We limited our study to this region of the atmosphere for two reasons. First, the predicted temperature changes due to doubled CO_2 are much larger in the stratosphere than in the troposphere. Second, longwave emission from the stratosphere is not complicated by the presence of clouds, which can introduce uncertainties in detecting the change in outgoing longwave flux due to increased CO_2 .

The clear sky excittance, or flux of energy in a given spectral interval, has been calculated for the 500 to 800 cm^{-1} region at the top of the atmosphere (3). We used the mid-latitude summer temperature and water vapor profiles of McClatchey *et al.* (4), assuming a maximum height of 50 km. Excittance was evaluated for each 5 cm^{-1} interval of the 500 to 800 cm^{-1} region. The transmissivities of CO_2 and the pure rotational band of water vapor were calculated from the band model of Malkmus (5). Transmissivity of the water vapor continuum was calculated from the formulation of Roberts *et al.* (6). All sensitivity studies have been carried out for a fixed water vapor profile (7).

Present-day excittance for the mid-latitude summer conditions, assuming a CO_2 mixing ratio of 320 ppm by volume, is shown in Fig. 1. The relatively low excittance in the spectral region between 620 and 720 cm^{-1} is emitted from the colder stratosphere. The peak centered at 667 cm^{-1} is due to emission by the fundamental band of CO_2 from the region of the stratosphere inversion, while the excittance outside 620 and 720 cm^{-1} is due mostly to radiative emission by tropospheric water vapor.

If the amount of atmospheric CO_2 is doubled to 640 ppm by volume, then for fixed tropospheric and stratospheric temperatures the total change in clear sky excittance at the top of the atmosphere in the 500 to 800 cm^{-1} spectral region is -2.7 W/m^2 . This is to be compared with a change of -2.2 W/m^2 when tropospheric and stratospheric temperatures are adjusted to their equilibrium values due to doubled CO_2 . The total outgoing flux for the entire longwave region, as measured by Vonder Haar and Suomi (8), is 230 W/m^2 . Thus, the percentage decrease in total emission when stratospheric and tropospheric temperatures are adjusted is only 0.96 percent. This change is fairly small and would be difficult to detect with current satellite instruments.

However, if we look at the percentage change in excittance due to doubled CO_2 for each narrow spectral interval, much

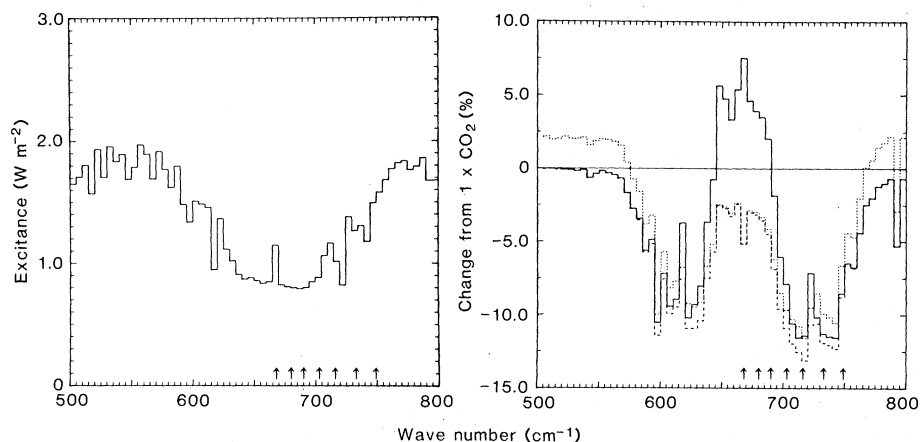


Fig. 1 (left). Excittance for mid-latitude summer conditions and a CO_2 mixing ratio of 320 ppm by volume. Arrows indicate the location of spectral channels for the HIRS instrument on the Tiros-N satellites. Fig. 2 (right). Percentage change in excittance due to doubled CO_2 . Changes are shown for the fixed temperature profile (case 1; continuous line), fixed tropospheric temperatures with reduced stratospheric temperatures (case 2; dashed line), and increased tropospheric temperatures with reduced stratospheric temperatures (case 3; dotted line). Arrows are the same as in Fig. 1.

larger changes occur. Three cases are used in Fig. 2 to illustrate the importance of looking at the change in excittance within small spectral intervals. In case 1 the temperature profile is held fixed for doubled CO_2 . Although this scenario is not predicted by climate models, it does illustrate the direct radiative forcing due to doubled CO_2 . In case 2 stratospheric temperatures are reduced, but tropospheric temperatures are held fixed. The perturbation of stratospheric temperatures, obtained from the model of Ramanathan and Dickinson (9), reflects stratospheric temperature decreases in agreement with other climate models. Case 3 in Fig. 2 represents the thermal response predicted by most climate models (10), wherein tropospheric temperatures are uniformly increased by 2.0 K while stratospheric temperatures are decreased in accordance with the second case.

The change in excittance for the fixed temperature case is positive for the spectral region between 620 and 690 cm^{-1} . This increase in emission comes from the upper stratosphere and leads to the decreased stratospheric temperatures of case 2. Outside this interval the excittance is decreased due to doubled CO_2 . The total change in this interval is -2.7 W/m^2 . In some intervals the change is larger than 10 percent. When stratospheric temperatures are decreased the excittance in each interval is decreased. The total change is -3.7 W/m^2 for this case. The region centered about 667 cm^{-1} indicates a decrease in excittance of 2.5 percent, while at the band center the decrease is 5 percent.

Case 3 differs from case 2 in only one respect. The increased tropospheric tem-

peratures lead to increased emission in the far wings of the spectral region. Increases on the order of 2.5 percent are indicated in these spectral regions. The largest changes in excittance are relatively insensitive to the particular climate scenario. This occurs because the emission around 620 and 720 cm^{-1} originates near the tropopause, where the temperature changes due to doubled CO_2 is small. Thus, these spectral regions are only an indication that CO_2 is increasing in the atmosphere. However, the spectral region centered at 668 cm^{-1} exhibits a substantial difference depending on changes in stratospheric temperature. This spectral region can be easily monitored by the high-resolution infrared radiation sounder (HIRS) instrument aboard the Tiros satellites (Fig. 1). Calculations similar to these have been repeated for summer and winter conditions at other latitudes. All the results indicate the same features shown in Fig. 2, although the absolute excittance differs from case to case.

We have shown that changes in excittance on the order of 5 percent in the spectral region of 667 cm^{-1} can be expected for a doubling of atmospheric CO_2 . However, we must now address the problem of whether this signal can be detected above noise arising from the particular instrument used for detection and noise due to the natural variability of the atmosphere.

Instrument noise does not pose a serious problem to detecting changes in excittance; for example, the root-mean-square error in radiance due to instrument noise on the Nimbus 3 satellite was about $0.25\text{ mW/m}^2\text{-sr-cm}^{-1}$, for a single observation (11). This implies an error in

excitance of about 0.004 W/m^2 . Since the error in instrument noise decreases as the square root of the number of samples (12), we are able to reduce this source of noise significantly below that of the signal we wish to detect. For example, about 100 northbound observations were made each day by Nimbus 3 (11). Thus, the daily error in excitance due to instrument noise was about 0.0004 W/m^2 , a value that places very little limitation on detection. A second source of instrument noise arises from using a series of different detectors over a long period. Each new satellite will carry a new instrument with different noise characteristics and, more importantly, a different absolute radiometric calibration. Solutions to this problem could involve looking at the ratio of the change between spectral channels, which might eliminate errors due to the calibration of the particular instrument, or using one instrument aboard the space shuttle over a long period. Thus we feel that errors due to the instrument will not severely limit the detection of changes in excitance.

Variations in the outgoing longwave flux due to the natural variability of the atmospheric thermal structure are also a source of noise. The standard deviations of radiance for the Nimbus 3 and Nimbus 6 satellites have been reported by Fritz and Soules (11) and Barnett (13), respectively. These studies indicate a standard deviation in radiance of $1 \text{ mW/m}^2\text{-sr}\text{-cm}^{-1}$, which corresponds to a standard deviation in excitance of 0.016 W/m^2 , for low and mid-latitudes in all months except December, January, and February. Higher latitudes (above 60°) exhibit much greater variability in radiance and would make detection of the signal due to increased CO_2 very difficult. Thus temporal averages should be confined to daily averaged measurements for non-winter months. Spatial averaging should not include latitudes above 60° in either hemisphere.

Figures 1 and 2 imply changes in excitance at 667 cm^{-1} of -0.06 W/m^2 . Thus the signal of change in excitance due to doubled CO_2 is about four times larger than the noise due to natural variability. This analysis has considered changes due to a doubling of atmospheric CO_2 ; obviously the natural variation will place limitations on the specific time in which a climatic signal is detectable, as is the case for any other detection method (2, 14).

This method for the 500 to 800 cm^{-1} spectral region can be used to detect changes in outgoing longwave flux, which in turn signify a change in the thermal structure of the stratosphere, in

CO_2 , or in both. Furthermore, perturbations of the stratospheric temperature structure are not only confined to increases in CO_2 . Increases in other trace gases can also affect the radiative balance of the atmosphere (2, 15). In particular, studies of reduced stratospheric ozone due to increases in chlorofluoromethanes (15) suggest that temperature decreases on the order of those due to doubled CO_2 may result. It is essential that other spectral regions be monitored in order to identify the causes of the observed changes in the atmosphere's thermal structure.

J. T. KIEHL

National Center for Atmospheric Research, Boulder, Colorado 80307

References and Notes

1. V. Gornitz, S. Lebedeff, J. Hansen, *Science* **215**, 1611 (1982); J. Hansen, D. Johnson, A. Lacis, S. Lebedeff, P. Lee, D. Rind, G. Russell, *ibid.* **213**, 957 (1981); G. Kukla and J. Gavin, *ibid.* **214**, 497 (1981).
2. R. A. Madden and V. Ramanathan, *ibid.* **209**, 763 (1980).
3. J. T. Houghton, *The Physics of the Atmosphere* (Cambridge Univ. Press, Cambridge, Mass., 1977), p. 149.
4. R. A. McClatchey, R. W. Fenn, J. E. A. Selby,

F. E. Volz, J. S. Garing, *U.S. Air Force Cambridge Res. Lab. Environ. Res. Pap. No. 254* (1971).

5. W. Malkmus, *J. Opt. Soc. Am.* **57**, 325 (1967).
6. R. E. Roberts, J. E. A. Selby, L. M. Biberman, *Appl. Opt.* **15**, 1085 (1976).
7. Calculations with two times the amount of water vapor for the doubled CO_2 cases change the results shown in Fig. 2 only slightly. The excitance due to tropospheric water vapor in the far spectral regions does not change since the lines in this region are saturated.
8. T. H. Vonder Haar and V. E. Suomi, *J. Atmos. Sci.* **28**, 305 (1971).
9. V. Ramanathan and R. E. Dickinson, *ibid.* **36**, 1084 (1979).
10. S. Manabe and R. T. Wetherald, *ibid.* **37**, 99 (1980); W. M. Washington and G. A. Meehl, *J. Geophys. Res.* **88**, 6600 (1983).
11. S. Fritz and S. D. Soules, *Mon. Weather Rev.* **100**, 582 (1972).
12. W. Mendenhall and R. L. Scheaffer, *Mathematical Statistics with Applications* (Duxbury, Belmont, Calif., 1973), pp. 185-191.
13. J. J. Barnett, *Philos. Trans. R. Soc. London Ser. A* **296**, 41 (1980).
14. E. S. Epstein, *J. Appl. Meteorol.* **21**, 1172 (1982).
15. V. Ramanathan, in *Interactions of Energy and Climate*, W. Bach, J. Pankrath, J. Williams, Eds. (Reidel, Boston, 1980), p. 269.
16. I thank V. Ramanathan for discussions which initiated this work. I also wish to thank W. W. Kellogg, W. Washington, and P. Chylek for helpful comments on an earlier draft of this manuscript. I am especially grateful for many stimulating discussions and helpful suggestions from J. A. Coakley, Jr. The National Center for Atmospheric Research is sponsored by the National Science Foundation.

16 May 1983

Determining the Solar Wind Speed Above Active Regions Using Remote Radio-Wave Observations

Abstract. *A new technique has made it possible to measure the velocity of portions of the solar wind during its flow outward from the sun. This analysis utilizes spacecraft (ISEE-3) observations of radio emission generated in regions of the solar wind associated with solar active regions. By tracking the source of these radio waves over periods of days, it is possible to measure the motion of the emission regions. Evidence of solar wind acceleration during this outward flow, consistent with theoretical models, has also been obtained.*

The spiral shape of the interplanetary magnetic field lines is a consequence of the outward flow of the solar wind and the solar rotation. Above about 10 solar radii (R_\odot), the magnetic field is carried out with the expanding plasma and its lines of force take a spiral shape first predicted by Parker (1; 2, pp. 41-72). This shape has been confirmed by in situ space probe measurements and also by radio tracking of solar energetic particles responsible for the type III burst radiation (3).

Solar type III radio bursts are produced by packets of energetic electrons that are accelerated in the low corona or chromosphere and travel outward through the corona and interplanetary space. At each altitude, the electrons excite plasma waves that are converted into electromagnetic waves at the plasma frequency or at its second harmonic (4).

During its first 4 years of operation, the ISEE-3 spacecraft (5) has been sta-

tioned close to the libration point situated ~ 240 earth radii toward the sun. This location is particularly good for radio observations since it is both far from the sources of the earth's radio noise and it allows almost continuous observations. The Paris Observatory-National Aeronautics and Space Administration Goddard Space Flight Center radio experiment on board the ISEE-3 spacecraft (6) uses the spin modulation of the received data resulting from the rotation of the spacecraft dipole antenna to deduce the direction of a compact radio source. The technique (3, 7) has been used to map the trajectories of intense isolated type III bursts through the interplanetary medium (3).

Hectometer-wavelength type III solar storms have been discovered during the last solar cycle as a result of RAE-1 (Radio Astronomy Explorer) satellite observations (8, 9). They consist of hundreds of individual type III storm bursts